

# HMR-1: Hierarchical Massage Robot with Vision-Language-Model for Embodied Healthcare

Rongtao Xu<sup>b,\*</sup>, Mingming Yu<sup>c,\*</sup>, Xiaofeng Han<sup>a,\*</sup>, Yu Zhang<sup>a</sup>, Kaiyi Hu<sup>d</sup>, Zhe Feng<sup>a</sup>, Zenghuang Fu<sup>a</sup>, Changwei Wang<sup>e</sup>, Weiliang Meng<sup>a,†</sup>, Xiaopeng Zhang<sup>a</sup>

<sup>a</sup>The State Key Laboratory of Multimodal Artificial Intelligence Systems, Institute of Automation, Chinese Academy of Sciences, China

<sup>b</sup>Spatiotemporal AI, China

<sup>c</sup>Hangzhou International Innovation Institute, Beihang University, China

<sup>d</sup>Georgia Institute of Technology, China

<sup>e</sup>Key Laboratory of Computing Power Network and Information Security, Ministry of Education; Shandong Computer Science Center, Qilu University of Technology (Shandong Academy of Sciences), China

arXiv:2603.08817v1 [cs.LG] 9 Mar 2026

## Abstract

The rapid advancement of Embodied Intelligence has opened transformative opportunities in healthcare, particularly in physical therapy and rehabilitation. However, critical challenges remain in developing robust embodied healthcare solutions, such as the lack of standardized evaluation benchmarks and the scarcity of open-source multimodal acupoint massage datasets. To address these gaps, we construct MedMessage-12K - a multimodal dataset containing 12,190 images with 174,177 QA pairs, covering diverse lighting conditions and backgrounds. Furthermore, we propose a hierarchical embodied massage framework, which includes a high-level acupoint grounding module and a low-level control module. The high-level acupoint grounding module uses multimodal large language models to understand human language and identify acupoint locations, while the low-level control module provides the planned trajectory. Based on this, we evaluate existing MLLMs and establish a benchmark for embodied massage tasks. Additionally, we fine-tune the Qwen-VL model, demonstrating the framework’s effectiveness. Physical experiments further confirm the practical applicability of the framework. Our dataset and code are publicly available at <https://github.com/Xiaofeng-Han-Res/HMR-1>.

**Keywords:** Embodied Intelligence, multimodal large language models, acupoint massage, healthcare robotics.

## 1. Introduction

Recent advancements in Multimodal Large Language Models (MLLMs)[1, 2, 3, 4, 5, 6] and Embodied AI[7, 8, 9, 10, 11, 12, 13, 14, 15, 16, 17] have demonstrated remarkable capabilities in complex reasoning, human intention understanding, and robotic manipulation[18, 19, 20]. Models such as LLaVA [21], Qwen-VL [22], and ManipLLM [23] have shown significant progress in integrating vision, language, and action, while robotics frameworks like RT-1 [24], RT-2 [25], and OpenVLA [26] leverage large-scale pretrained models to directly predict robot actions. These breakthroughs suggest that embodied intelligence could transform domains requiring precise human-machine interaction.

Healthcare is one of the most promising application areas, particularly in physical therapy and rehabilitation. Intelligent systems can assist or even replace human therapists in repetitive and precise procedures, such as acupoint massage. However, developing robust embodied healthcare solutions remains challenging[27, 28, 29]. Current intelligent systems achieve

strong results in passive tasks such as medical QA or imaging analysis, but struggle in treatment scenarios that demand active physical interaction and fine-grained grounding. Existing frameworks often rely on pre-programmed trajectories and fail to translate natural language into precise embodied actions[30, 31, 32, 33].

A straightforward alternative would be to adopt traditional object detection frameworks (e.g., Faster R-CNN [34], YOLO[35], RT-DETR[36]) for acupoint localization. Yet, these detectors are designed for static category prediction and bounding-box regression, making them inadequate for understanding complex human instructions. In acupoint massage, commands often involve both semantic interpretation and action grounding (e.g., “locate the Zusanli acupoint and apply moderate pressure”). Traditional detectors cannot align linguistic intent with visual perception, thus limiting their applicability. We aim to overcome this gap by leveraging MLLMs, which inherently combine language comprehension, visual grounding, and reasoning, enabling instruction-driven embodied massage.

To address these challenges, we introduce **MedMessage-12K**, a multimodal dataset containing 12,190 images and 174,177 QA pairs under diverse lighting and background conditions, specifically designed for acupoint massage tasks. Build-

\*Equal contribution.

†Corresponding authors.

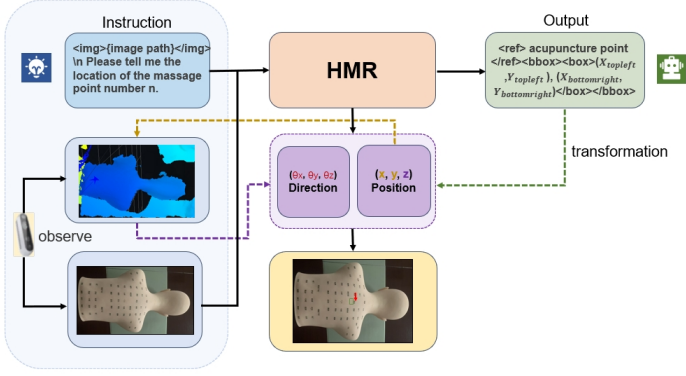


Figure 1: The proposed HMR framework. Given a textual instruction and an RGB-D observation, the model predicts the 6-DOF end-effector pose for robotic massage.

ing on this dataset, we propose a hierarchical embodied massage framework with two core components: (i) a high-level acupoint grounding module that employs MLLMs to understand natural language and localize acupoints, and (ii) a low-level control module that generates precise trajectories for robotic execution. **Our primary contributions are as follows:**

- **Dataset Construction:** We construct MedMessage-12K, the first large-scale multimodal dataset for embodied massage, providing a foundation for training and evaluation.
- **Framework Development:** We propose a hierarchical framework that bridges natural language understanding and robotic control, enabling precise acupoint localization and safe operations.
- **Model Benchmarking and Fine-Tuning:** We evaluate existing MLLMs and establish a benchmark for embodied massage tasks, and fine-tune Qwen-VL to validate our approach.
- **Physical Validation:** We conduct real-world experiments with a Franka Panda robot, demonstrating the framework’s reliability and generalizability.

## 2. Related Work

### 2.1. Embodied AI

Traditional robotic motion control [37, 38] has primarily relied on state-based reinforcement learning for training. Subsequently, several studies have incorporated visual observations as inputs to enhance the understanding of complex environments [12, 39, 40]. For instance, Where2Act [41] utilizes visual observations to predict actionable regions of objects, while AnyGrasp [42] employs point cloud data for learning grasping poses. Inspired by the advancements in MLLMs, recent works have proposed vision-language-action models tailored for robotic manipulation. For example, ManipLLM [23] introduces a three-level instruction fine-tuning framework to endow MLLMs with manipulation capabilities, and SC-MLLM [43] incorporates a correction mechanism to improve performance. Additionally, RoboMamba [7] leverages the Mamba

architecture to enhance model efficiency. Models such as RT-1 [24], RT-2 [25], and OpenVLA [26] directly fine-tune large pretrained MLLMs to predict robot actions using the Open X-Embodiment dataset [44]. In contrast to these approaches, our work focuses on advancing the application of MLLMs in embodied massage scenarios, aiming to address the unique challenges and requirements of this domain.

### 2.2. Multimodal Large Language Models

Recent advancements in large language models (LLMs) [2, 3] have demonstrated remarkable capabilities in complex reasoning and human intention understanding. To further enhance their multimodal comprehension, several studies, such as LLaVA [21], Qwen-VL [22], and Videollama [22], have begun to fine-tune these models using multimodal data for multimodal learning. These models have seen increasing adoption in various applications, including visual dialogue, scene understanding, and robotic task planning. Despite the considerable performance improvements in MLLMs, their embodied massage capabilities remain underexplored. Consequently, we propose a hierarchical embodied massage model designed to enhance the performance of MLLMs in embodied medical scenarios.

### 2.3. Open-Source Datasets for Embodied Healthcare

Open-source datasets play a pivotal role in advancing embodied healthcare technologies, offering critical resources for research and innovation despite their current limitations. Key datasets such as CaDIS[27], which provides annotated video images for cataract surgery and supports semantic segmentation for computer-assisted surgery systems, and MEDQA[29], which offers a diverse range of medical exam questions to enhance natural language processing-based medical question-answering systems, have significantly contributed to the field. Additionally, multimodal datasets like MedTrinity-25M[28], with over 25 million richly annotated medical images, enable tasks such as image classification, visual question answering, and report generation, fostering the development of multimodal models for complex diagnostics and patient care. These datasets primarily concentrate on general medical image segmentation and medical question-answering tasks. However, for acupoint massage tasks, there is currently a lack of large-scale, open-source multimodal datasets. To bridge this gap, we propose a novel dataset focused on acupoint-related data, aiming to advance research in embodied massage tasks and contribute to the development of intelligent healthcare systems.

## 3. Method

### 3.1. Task Definition

The embodied massage task requires a robotic system to understand high-level natural language instructions, precisely localize acupoints, and plan safe robotic motions. Formally, given a textual command  $\mathcal{T}$  (e.g., “Locate the Zusanli acupoint and apply moderate pressure”) with multimodal inputs ( $I_{\text{RGB}} \in \mathbb{R}^{W \times H \times 3}$ ,  $I_{\text{Depth}} \in \mathbb{R}^{W \times H}$ ), the system must generate a collision-free 6-DOF end-effector pose  $\mathbf{p} =$

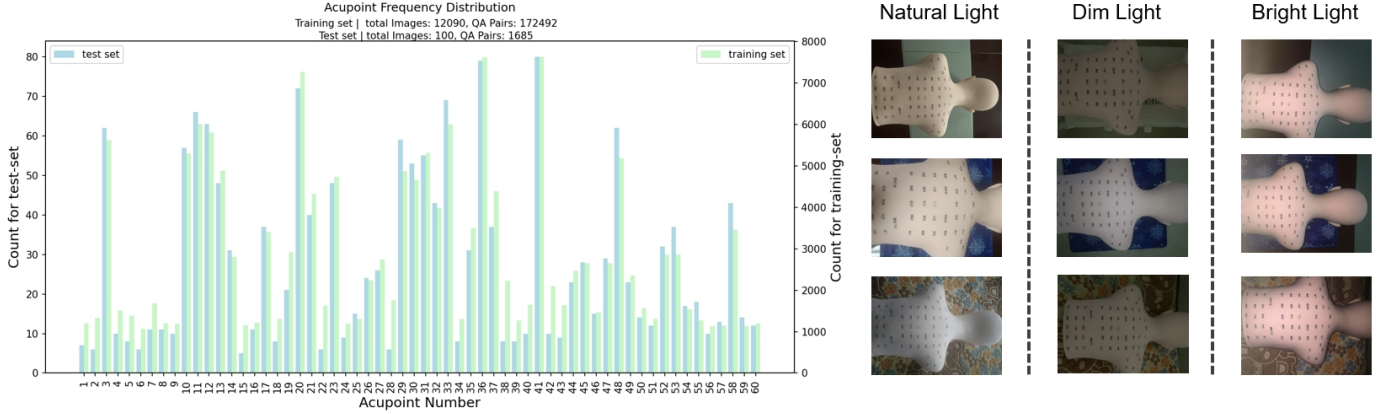


Figure 2: The bar chart on the left shows the distribution of acupoints in the test set and training set, while the right side displays images of the mannequin with acupoints under different lighting and background conditions.

$(x, y, z, \theta_x, \theta_y, \theta_z) \in \mathbb{R}^3 \times \mathbb{SO}(3)$  for the Franka Emika Panda robot. This pose integrates both positional coordinates  $\mathbf{a}_{\text{pos}} \in \mathbb{R}^3$  and directional orientation  $\mathbf{a}_{\text{dir}} \in \mathbb{R}^{3 \times 3}$ . The task inherently bridges natural language understanding, visual perception, and robotic control for real-world human-robot collaboration.

### 3.2. Data Collection and Augmentation

We introduce MedMessage-12K, the first large-scale multi-modal dataset for hierarchical massage manipulation learning, which consists of 1,030 acupoint images of medical dummies and 15,092 annotated question and answer (QA) pairs. The dataset includes images from diverse backgrounds and lighting conditions (e.g., Natural, Dim, Bright), ensuring it covers a wide range of environments to promote generalization (as shown in Figure 2). In terms of acupoint distribution, the dataset covers 60 different massage points. Figure 2 illustrates the distribution in training and test sets. The frequency of each acupoint varies between them, better reflecting real-world demand and ensuring diversity and representativeness. For convenience, we map acupoint names to numerical indices, and in the subsequent text, denote names by IDs. To enhance diversity and robustness, we applied data augmentation, focusing on generalization across position and height. Using geometric transformations such as random cropping and rotations, we generated additional training data. These augmentations enriched the dataset, increasing the images to 12,190 and QA pairs to 174,177. This not only improved generalization across lighting and backgrounds but also enhanced adaptability to positions and heights, ensuring effective reasoning in real-world scenarios. The final dataset composition, as shown in Table 1, includes both annotated and augmented data for training and testing. This dataset provides the foundation for evaluating embodied models for healthcare interventions.

### 3.3. System Overview

In this section, we demonstrate how we enable MLLMs to possess acupoint massage capabilities. As depicted in Fig 3, our architecture consists of two core components: (1) a High-Level

Table 1: MedMessage-12K Dataset Composition

Category	Partition	Images	QA Pairs
Training Set	Annotated Data	930	13,407
	Augmented Data	12,090	172,492
Test Set	Annotated Data	100	1,685

Grounding Module (HLGM) for semantic interpretation of human instructions and acupoint localization, and (2) a Low-Level Control Module (LLCM) that translates spatial coordinates into kinematic control signals.

#### 3.3.1. High-Level grounding Module

For the high-level grounding model, we employ the pre-trained  $Q_{\text{wen-VL}}$  [22]. The textual instruction  $T$  is encoded into textual features using the tokenizer of the pre-trained  $Q_{\text{wen}}$  model. Given an RGB image  $I \in \mathbb{R}^{H \times W \times 3}$ , we utilize OpenCLIP ViT-bigG [45] as the visual feature extractor to obtain visual representations. Subsequently, a single-layer cross-attention module serves as the vision-language adaptor. This module employs a set of trainable vectors as queries and the image features as keys for cross-attention operations, effectively compressing the image features. Following this, the  $Q_{\text{wen-7B}}$  model acts as the LLM decoder to generate the final response. As illustrated in the Fig 3, we freeze the visual encoder during training and only fine-tune the vision-language adaptor and the language model. The outputs of the model are supervised using the cross-entropy loss function.

During training, we utilize augmented data consisting of 172,492 QA pairs to train our model. Following the design of  $Q_{\text{wen-VL}}$ , we use special tokens to distinguish between different types of information. For the input, we adopt the special token  $\langle \text{img} \rangle$  to differentiate between image inputs and text inputs. For the output, to enhance the model’s fine-grained understanding and grounding capabilities for massage points, we use special tokens  $\langle \text{box} \rangle$  and  $\langle / \text{box} \rangle$  to demarcate bounding box coordinates, and  $\langle \text{ref} \rangle$  and  $\langle / \text{ref} \rangle$  to associate bounding boxes with their corresponding descriptive words or sen-

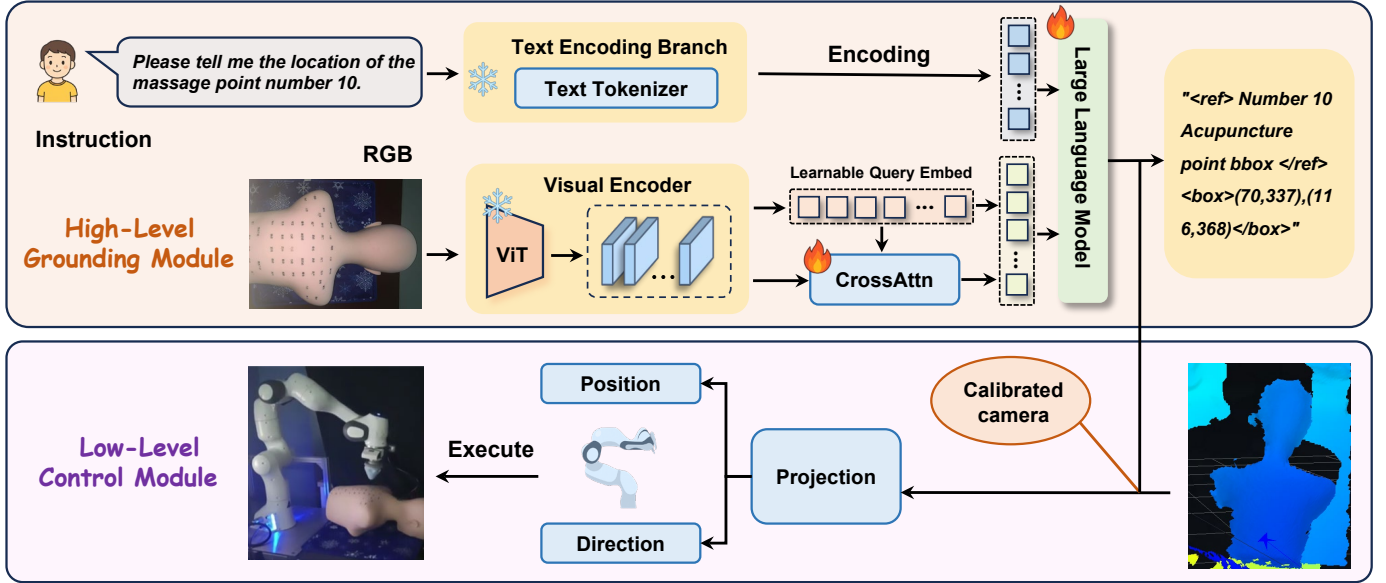


Figure 3: System architecture of the proposed framework, consisting of a High-Level Grounding Module (HLGM) and a Low-Level Control Module (LLCM).

tences. For any acupuncture point, the bounding box coordinates are normalized within the range  $[0, 1000]$ . These tokens ensure accurate localization and description of target regions, such as specific massage points in an image. The input and output format can be summarized as follows:

**Input:** `<img>{image}</img>{instruction_content}`  
**Output:** `<ref> {acupuncture point} bbox</ref><box>(Xtop_left,Ytop_left),(Xbottom_right,Ybottom_right)</box>`

### 3.3.2. Low-Level control Module

In this approach, the MLLM is first used to process the input 2D image and extract the 2D coordinates of the acupoint locations in the image. Then, a depth map of the scene is obtained using a depth camera, which provides the actual distance from the camera to each pixel. By utilizing the depth camera's intrinsic and extrinsic parameters, along with the depth information, the 2D pixel coordinates in the image can be transformed into corresponding 3D point cloud coordinates, namely position  $(x, y, z)$ . These points can be used for plane fitting. We can apply the RANSAC algorithm to extract a plane model from the point cloud data, and subsequently obtain the normal vector of the plane. Next, we calculate the angle between the fitted plane's normal vector and the reference plane's normal vector using their dot product. Finally, by utilizing the "vertical tapping principle," we can deduce the object's rotational posture based on the change in the plane's normal vector, thereby obtaining the direction. Combining this with the previously obtained position  $(x, y, z)$ , we can obtain the complete pose  $p = (x, y, z, \theta_x, \theta_y, \theta_z)$ .

After obtaining the target's pose  $p = (x, y, z, \theta_x, \theta_y, \theta_z)$ , the robotic arm calculates the corresponding joint configurations using Inverse Kinematics (IK) algorithms to move the end-effector to the target position while maintaining the correct

orientation. This step ensures that the arm can accurately reach the target and perform precise operations. Next, the robotic arm uses the polynomial fitting to plan a collision-free path from the current joint configuration to the target position. Based on the path planning, the robotic arm generates a smooth trajectory using spline interpolation to ensure that the movement process does not involve abrupt acceleration or velocity changes. After trajectory generation, the robotic arm incorporates feedback control during execution to ensure it follows the planned trajectory. Finally, the robotic arm reaches the acupoint position and performs the massage operation.

## 4. Experiments

### 4.1. Acupoint Grounding Success Rate Across Models

To evaluate the acupoint localization capabilities of existing MLLMs, we conducted comprehensive tests on Qwen-VL-Max and GPT-4o using the following standardized input instruction:

**Prompt:**

The coordinate system defines the top-left corner as  $(0,0)$  and the bottom-right corner as  $(1000,1000)$ . Please output the bounding box coordinates for the acupuncture point {acupoint name} in the format: `<box>(xleft top}, yleft top}, (xright bottom}, yright bottom)</box>`. Provide only the final answer without intermediate reasoning.

Table 2: Acupoint grounding success across IoU thresholds.

Model	Grounding Success Rate		
	IoU=0.3	IoU=0.5	IoU=0.75
Qwen-VL-Max	0.12%	0%	0%
GPT-4o	0.59%	0.07%	0%
Our Model	87.60%	81.42%	67.77%

As shown in Table 2, current multimodal large language models demonstrate significant limitations in acupoint grounding tasks. Both GPT-4o and Qwen-VL-Max exhibit grounding success rates approaching 0% across various IoU thresholds, indicating their lack of fine-grained perception capability for massage acupoints. In contrast, our proposed model achieves substantially higher grounding success rates of 87.60%, 81.42%, and 67.77% at IoU thresholds of 0.3, 0.5, and 0.75 respectively, demonstrating superior precision in acupoint localization tasks.

## 4.2. Ablation study

### 4.2.1. Impact of Data Scale on Model Performance

In this section, we analyze the impact of data scale on model performance. We train the model using subsets of the annotated training data, specifically 10%, 20%, 40%, 70%, and 100% of the original and augmented samples, and evaluate the performance on the same test set.

**Table 3:** Impact of the Data Scale.

Data	Grounding Success Rate		
	IoU=0.3	IoU=0.5	IoU=0.75
10%	47.18%	37.45%	26.17%
20%	61.60%	51.10%	39.17%
40%	75.25%	66.83%	53.41%
70%	83.03%	75.91%	62.49%
100%	87.60%	81.42%	67.77%

Our experimental results demonstrate a clear trend: the model’s performance consistently improves as the data scale increases, as shown in Table 3. For instance, at an IoU threshold of 0.3, the test accuracy rises from 47.18% with 10% of the data to 87.60% with the full dataset. Similar improvements are observed at higher IoU thresholds (0.5 and 0.75), indicating that larger datasets enhance the model’s ability to localize acupoints with greater precision. However, the incremental gains diminish as the data scale grows, particularly when moving from 70% to 100% of the dataset. This suggests that while increasing data volume is beneficial, the diversity and quality of the data also play a critical role in achieving further performance improvements. These findings highlight the importance of both data scale and diversity in developing robust models for acupoint localization tasks.

### 4.2.2. Impact of Data Augmentation

To evaluate the effectiveness of our data augmentation strategy, we conduct experiments with and without data augmentation. The results, as shown in Table 4, demonstrate a significant improvement in grounding success rates when data augmentation is applied.

Without data augmentation, the grounding success rates are 60.89%, 48.96%, and 35.54% for IoU thresholds of 0.3, 0.5, and 0.75, respectively. With data augmentation, these rates increase significantly to 87.60%, 81.42%, and 67.77% for the same thresholds. This represents performance improvements of 26.71 at IoU=0.3, 32.46 at IoU=0.5, and 32.23 at IoU=0.75.

**Table 4:** Grounding Success Rate w/ and w/o Data Aug.

Data	Grounding Success Rate		
	IoU=0.3	IoU=0.5	IoU=0.75
w/o data augmentation	60.89%	48.96%	35.54%
W data augmentation	87.60%	81.42%	67.77%

The substantial gains highlight the critical role of data augmentation in enhancing the model’s ability to generalize and accurately localize acupoints under diverse conditions.

### 4.3. Massage in Real-World Environments

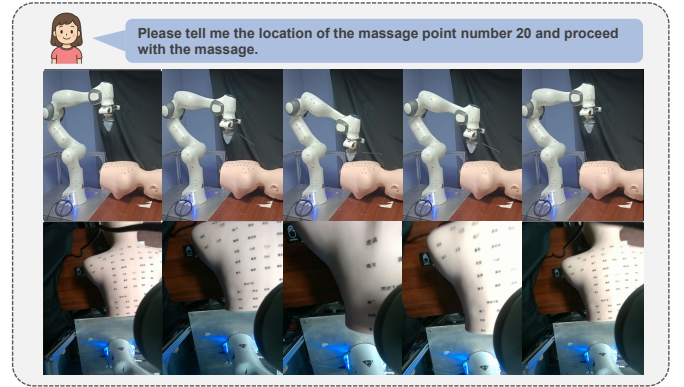


**Figure 4:** Massage in real-world environments: first-person RGB and third-person frames of robot execution.

To further evaluate the generalizability of our framework, we conduct experiments in real-world environments. We use a Franka Panda Robot equipped with a massage ball as the actuator and a RealSense D455 camera to capture RGB and depth images. The HMR model is deployed on a computer with an NVIDIA A6000 GPU. As demonstrated in Fig 4, our model can accurately locate and perform massage on specified acupuncture points under varying lighting conditions and backgrounds, showcasing the robustness and generalizability of our approach.

## 5. Conclusions

In this work, we address key challenges in embodied intelligence for healthcare by introducing a hierarchical framework and a large-scale multimodal dataset for acupoint massage tasks. Our framework integrates a high-level grounding module for acupoint localization and a low-level control module for trajectory planning. We evaluate and fine-tune multimodal large language models, demonstrating strong generalization across diverse conditions. Physical experiments validate the framework’s practical applicability, paving the way for robust and scalable healthcare solutions.

## References

- [1] X. Han, S. Chen, Z. Fu, Z. Feng, L. Fan, D. An, C. Wang, L. Guo, W. Meng, X. Zhang, R. Xu, S. Xu, Multimodal

- fusion and vision–language models: A survey for robot vision, *Information Fusion* 126 (2026) 103652.
- [2] H. Touvron, T. Lavril, G. Izacard, X. Martinet, M.-A. Lachaux, T. Lacroix, B. Roziere, N. Goyal, E. Hambro, F. Azhar, et al., Llama: Open and efficient foundation language models, arXiv preprint arXiv:2302.13971 (2023).
- [3] L. Floridi, M. Chiriatti, Gpt-3: Its nature, scope, limits, and consequences, *Minds and Machines* 30 (2020) 681–694.
- [4] A. Hurst, A. Lerer, A. P. Goucher, A. Perelman, A. Ramesh, A. Clark, A. Ostrow, A. Welihinda, A. Hayes, A. Radford, et al., Gpt-4o system card, arXiv preprint arXiv:2410.21276 (2024).
- [5] Y. Jin, J. Li, T. Gu, Y. Liu, B. Zhao, J. Lai, Z. Gan, Y. Wang, C. Wang, X. Tan, et al., Efficient multimodal large language models: A survey, *Visual Intelligence* 3 (1) (2025) 27.
- [6] J. Yang, S. Yang, A. W. Gupta, R. Han, L. Fei-Fei, S. Xie, Thinking in space: How multimodal large language models see, remember, and recall spaces, in: *Proceedings of the Computer Vision and Pattern Recognition Conference, 2025*, pp. 10632–10643.
- [7] J. Liu, M. Liu, Z. Wang, et al., Robomamba: Efficient vision-language-action model for robotic reasoning and manipulation, *Advances in Neural Information Processing Systems* 37 (2025) 40085–40110.
- [8] K. Black, N. Brown, D. Driess, A. Esmail, M. Equi, C. Finn, N. Fusai, L. Groom, K. Hausman, B. Ichter, et al.,  $\pi 0$ : A vision-language-action flow model for general robot control. corr, abs/2410.24164, 2024. doi: 10.48550, arXiv preprint ARXIV.2410.24164.
- [9] Z. Hou, T. Zhang, Y. Xiong, H. Duan, H. Pu, R. Tong, C. Zhao, X. Zhu, Y. Qiao, J. Dai, et al., Dita: Scaling diffusion transformer for generalist vision-language-action policy, arXiv preprint arXiv:2503.19757 (2025).
- [10] R. Xu, H. Gao, M. Yu, D. An, S. Chen, C. Wang, L. Guo, X. Liang, S. Xu, 3d-more: Unified modal-contextual reasoning for embodied question answering, arXiv preprint arXiv:2507.12026 (2025).
- [11] S. Liu, L. Wu, B. Li, H. Tan, H. Chen, Z. Wang, K. Xu, H. Su, J. Zhu, Rdt-1b: a diffusion foundation model for bimanual manipulation, arXiv preprint arXiv:2410.07864 (2024).
- [12] J. Zhang, K. Wang, R. Xu, G. Zhou, Y. Hong, X. Fang, Q. Wu, Z. Zhang, W. He, Navid: Video-based vlm plans the next step for vision-and-language navigation, arXiv preprint arXiv:2402.15852 (2024).
- [13] B. Lin, Y. Nie, K. L. Zai, Z. Wei, M. Han, R. Xu, M. Niu, J. Han, L. Lin, C. Lu, et al., Evolgenav: Self-improving embodied reasoning for llm-based vision-language navigation, arXiv preprint arXiv:2506.01551 (2025).
- [14] Z. Zhang, W. Zhu, H. Pan, X. Wang, R. Xu, X. Sun, F. Zheng, ActiveVln: Towards active exploration via multi-turn rl in vision-and-language navigation, arXiv preprint arXiv:2509.12618 (2025).
- [15] Y. Yan, R. Xu, J. Zhang, P. Li, X. Liang, J. Yin, Instrugen: Automatic instruction generation for vision-and-language navigation via large multimodal models, arXiv preprint arXiv:2411.11394 (2024).
- [16] J. Lin, H. Gao, X. Feng, R. Xu, C. Wang, M. Zhang, L. Guo, S. Xu, Advances in embodied navigation using large language models: A survey, arXiv preprint arXiv:2311.00530 (2023).
- [17] W. Huang, C. Wang, Y. Li, R. Zhang, L. Fei-Fei, Rekep: Spatio-temporal reasoning of relational keypoint constraints for robotic manipulation, arXiv preprint arXiv:2409.01652 (2024).
- [18] R. Xu, J. Zhang, M. Guo, Y. Wen, H. Yang, M. Lin, J. Huang, Z. Li, K. Zhang, L. Wang, et al., A0: An affordance-aware hierarchical model for general robotic manipulation, in: *Proceedings of the IEEE/CVF International Conference on Computer Vision, 2025*, pp. 13491–13501.
- [19] K. Zhang, R. Xu, P. Ren, J. Lin, H. Wu, L. Lin, X. Liang, Robridge: A hierarchical architecture bridging cognition and execution for general robotic manipulation, arXiv preprint arXiv:2505.01709 (2025).
- [20] L. Ma, J. Wen, M. Lin, R. Xu, X. Liang, B. Lin, J. Ma, Y. Wang, Z. Wei, H. Lin, et al., Phylblock: A progressive benchmark for physical understanding and planning via 3d block assembly, arXiv preprint arXiv:2506.08708 (2025).
- [21] H. Liu, C. Li, Q. Wu, Y. J. Lee, Visual instruction tuning, arXiv preprint arXiv:2304.08485 (2023).
- [22] P. Wang, S. Bai, S. Tan, et al., Qwen2-vl: Enhancing vision-language model’s perception of the world at any resolution, arXiv preprint arXiv:2409.12191 (2024).
- [23] X. Li, M. Zhang, Y. Geng, et al., Manipllm: Embodied multimodal large language model for object-centric robotic manipulation, in: *Proceedings of the IEEE/CVF Conference on Computer Vision and Pattern Recognition, 2024*, pp. 18061–18070.
- [24] A. Brohan, N. Brown, J. Carbajal, et al., Rt-1: Robotics transformer for real-world control at scale, arXiv preprint arXiv:2212.06817 (2022).

- [25] A. Brohan, N. Brown, J. Carbajal, Y. Chebotar, X. Chen, K. Choromanski, T. Ding, D. Driess, A. Dubey, C. Finn, et al., Rt-2: Vision-language-action models transfer web knowledge to robotic control, arXiv preprint arXiv:2307.15818 (2023).
- [26] M. Kim, K. Pertsch, S. Karamcheti, et al., Openvla: An open-source vision-language-action model, arXiv preprint arXiv:2406.09246 (2024).
- [27] M. Grammatikopoulou, E. Flouty, A. Kadkhodamohammadi, G. Quellec, A. Chow, J. Nehme, I. Luengo, D. Stoyanov, Cadis: Cataract dataset for surgical rgb-image segmentation, *Medical Image Analysis* 71 (2021) 102053.
- [28] Y. Xie, C. Zhou, L. Gao, J. Wu, X. Li, H.-Y. Zhou, S. Liu, L. Xing, J. Zou, C. Xie, et al., Medtrinity-25m: A large-scale multimodal dataset with multigranular annotations for medicine, arXiv preprint arXiv:2408.02900 (2024).
- [29] K. Singhal, S. Azizi, T. Tu, S. S. Mahdavi, J. Wei, H. W. Chung, N. Scales, A. Tanwani, H. Cole-Lewis, S. Pfohl, et al., Large language models encode clinical knowledge, *Nature* 620 (7972) (2023) 172–180.
- [30] M. Cleary, S. West, D. McGarry, M. Greenwood, R. Kornhaber, Manipulation in health care: A positive or negative experience?, *Issues in Mental Health Nursing* 40 (11) (2019) 985–987.
- [31] J. R. Chapman, K. Wiechert, J. C. Wang, Evidence-based medicine, media, and manipulation (2018).
- [32] A. Longhini, Y. Wang, I. Garcia-Camacho, D. Blanco-Mulero, M. Moletta, M. Welle, G. Alenyà, H. Yin, Z. Erickson, D. Held, et al., Unfolding the literature: A review of robotic cloth manipulation, *Annual Review of Control, Robotics, and Autonomous Systems* 8 (1) (2025) 295–322.
- [33] J. Ye, S. Bronstein, J. Hai, M. A. Hashish, Deepseek in healthcare: a survey of capabilities, risks, and clinical applications of open-source large language models, arXiv preprint arXiv:2506.01257 (2025).
- [34] S. Ren, K. He, R. Girshick, J. Sun, Faster r-cnn: Towards real-time object detection with region proposal networks, *Advances in neural information processing systems* 28 (2015).
- [35] R. Khanam, M. Hussain, Yolov11: An overview of the key architectural enhancements, arXiv preprint arXiv:2410.17725 (2024).
- [36] Y. Zhao, W. Lv, S. Xu, J. Wei, G. Wang, Q. Dang, Y. Liu, J. Chen, Detsr beat yolos on real-time object detection, in: *Proceedings of the IEEE/CVF conference on computer vision and pattern recognition*, 2024, pp. 16965–16974.
- [37] S. Joshi, S. Kumra, F. Sahin, Robotic grasping using deep reinforcement learning, in: *2020 IEEE 16th International Conference on Automation Science and Engineering (CASE)*, IEEE, 2020, pp. 1461–1466.
- [38] M. Andrychowicz, B. Baker, M. Chociej, R. Jozefowicz, B. McGrew, J. Pachocki, A. Petron, M. Plappert, G. Powell, A. Ray, et al., Learning dexterous in-hand manipulation, *The International Journal of Robotics Research* 39 (1) (2020) 3–20.
- [39] R. Xu, J. Zhang, J. Sun, C. Wang, Y. Wu, S. Xu, W. Meng, X. Zhang, Mrftrans: Multimodal representation fusion transformer for monocular 3d semantic scene completion, *Information Fusion* (2024) 102493.
- [40] R. Xu, C. Wang, D. Zhang, M. Zhang, S. Xu, W. Meng, X. Zhang, Deffusion: Deformable multimodal representation fusion for 3d semantic segmentation, in: *2024 IEEE International Conference on Robotics and Automation (ICRA)*, IEEE, 2024, pp. 7732–7739.
- [41] K. Mo, L. J. Guibas, M. Mukadam, A. Gupta, S. Tulsiani, Where2act: From pixels to actions for articulated 3d objects, in: *Proceedings of the IEEE/CVF International Conference on Computer Vision*, 2021, pp. 6813–6823.
- [42] H.-S. Fang, C. Wang, H. Fang, M. Gou, J. Liu, H. Yan, W. Liu, Y. Xie, C. Lu, Anygrasp: Robust and efficient grasp perception in spatial and temporal domains, *IEEE Transactions on Robotics* (2023).
- [43] J. Liu, C. Li, G. Wang, et al., Self-corrected multimodal large language model for robot manipulation and reflection, *Journal Name* (2023).
- [44] Q. Vuong, S. Levine, H. R. Walke, K. Pertsch, A. Singh, R. Doshi, C. Xu, J. Luo, L. Tan, D. Shah, et al., Open x-embodiment: Robotic learning datasets and rt-x models, in: *Towards Generalist Robots: Learning Paradigms for Scalable Skill Acquisition@ CoRL2023*, 2023.
- [45] A. Radford, J. W. Kim, C. Hallacy, A. Ramesh, G. Goh, S. Agarwal, G. Sastry, A. Askell, P. Mishkin, J. Clark, et al., Learning transferable visual models from natural language supervision, in: *International conference on machine learning*, PmlR, 2021, pp. 8748–8763.